Tunable band gaps in acoustic metamaterials with periodic arrays of resonant shunted piezos*

Chen Sheng-Bing(陈圣兵)†, Wen Ji-Hong(温激鸿), Wang Gang(王 刚), and Wen Xi-Sen(温熙森)

Laboratory of Science and Technology on Integrated Logistics Support, National University of Defense Technology, Changsha 410073, *China*
Key Laboratory of Photonic and Phononic Crystal of Ministry of Education, National University of Defense Technology, Changsha 410073, *China*

(Received 25 September 2012; revised manuscript received 14 November 2012)

Periodic arrays of resonant shunted piezoelectric patches are employed to control the wave propagation in a two-dimensional (2D) acoustic metamaterial. The performance is characterized by the finite element method. More importantly, we propose an approach to solving the conventional issue of the nonlinear eigenvalue problem, and give a convenient solution to the dispersion properties of 2D metamaterials with periodic arrays of resonant shunts in this article. Based on this modeling method, the dispersion relations of a 2D metamaterial with periodic arrays of resonant shunted piezos are calculated. The results show that the internal resonances of the shunting system split the dispersion curves, thereby forming a locally resonant band gap. However, unlike the conventional locally resonant gap, the vibrations in this locally resonant gap are unable to be completely localized in oscillators consisting of shunting inductors and piezo-patches.

Keywords: piezoelectric shunting, metamaterial, phononic, band gaps

PACS: 43.20+g, 43.40+s, 02.60.–x, 77.65.–g **DOI:** 10.1088/1674-1056/22/7/074301

1. Introduction

Elastic wave propagation in periodic structures have been studied for many years.[1–3] The vibration response of a periodic structure has been applied primarily to pass band and stop band analysis. Recently, the propagation of elastic or acoustic waves in a periodic metamaterial called phononic crystal (PC) has received considerable attention.[4–12] There are two kinds of gap formation mechanisms for PCs, i.e., Bragg scattering mechanism and locally resonant (LR) mechanism. The studies have shown that the existence of the Bragg gap is strongly related to a large acoustic impedance ratio between the scatterers and the matrix. The central frequencies are always given by Bragg's condition $f = n\,(v/2a)$ $(n = 1, 2, 3\ldots)$, where v is the elastic velocity of the matrix material and a is the lattice constant. The pioneering work of Liu *et al.*[6] has opened additional fields of PCs. The authors studied three-dimensional PCs consisting of cubic arrays of coated lead spheres immersed in an epoxy matrix, and proposed a new kind of gap formation mechanism, i.e., LR. The resonances of scatter units are the dominant factor in the formation of LR gaps. More recently, the development of LR PCs has been extended to a newly emerging field: acoustic metamaterials.[13–16] Acoustic metamaterials are generally regarded as the material with manmade microstructure that possesses unusual physical behaviors such as band gap, negative refraction, acoustic cloaking, etc.

Similarly, structure periodically shunted by an electrical circuit can also produce the LR band gap. Moreover, the tunable characteristics of a shunted piezo-patch allow the band gap to be tuned in a desired frequency range. Thorp *et al.*[17,18] used a periodic array of RL-shunted piezos mounted on a rod and fluid-loaded shells to create band gaps centered at the tuning frequency of the shunting circuit. Airold and Ruzzene[19] used multi-resonant shunts to generate multiple LR band gaps in a beam. Subsequently, they proposed the design of one-dimensional tunable acoustic metamaterial through periodic arrays of resonant shunted piezos.[20] The authors also carried out a lot of theoretical and experimental investigations on phononic rods[21] and beams[22–26] with shunting circuits, and obtained some helpful conclusions. These studies demonstrate how resonant piezoelectric shunts can be utilized to affect the equivalent mechanical properties of an elastic waveguide and therefore suggest their applications in developing tunable band gaps. Though this strategy has been extended to flat plates hosting periodic arrays of RL-shunted piezo-patches[27,28] for two years, little progress has been reported. The reason for this is that no effective modeling method has been proposed so far to predict the dispersion properties in an arbitrary direction, though Spadoni *et al.*[27] have generalized the transfer matrix method to calculate the dispersion relations of waves propagating in some specific directions. They pointed out that the resulting dynamic stiffness matrix of the finite element approach is a complicated function of frequency, so that the conventional method of specifying the wave vector and solving frequency is not applicable in this case.

In this paper, we propose an effective method to circumvent the aforementioned complicated dynamic stiffness matrix and obtain the dispersion relations of waves propagating in an

*Project supported by the National Natural Science Foundation of China (Grant Nos. 50905182 and 51175501).
†Corresponding author. E-mail: nudt_chen@163.com
© 2013 Chinese Physical Society and IOP Publishing Ltd

arbitrary direction conveniently. Based on this improved modeling method, the band structure of the two-dimensional (2D) metamaterial with periodic arrays of resonant shunted piezos is calculated. Specifically, the vibration modes corresponding to the edge frequencies of the band gap induced by internal resonance of shunting system are studied and compared with conventional LR gaps in detail.

2. Improved finite element modeling

2.1. Configuration

The 2D acoustic metamaterial consists of a substrate plate and arrays of shunted piezoelectric patches, which are oppositely bonded to the upper and lower surfaces of the plate as shown in Fig. 1. The periodic plate behaves as a tunable 2D waveguide propagating transverse waves. The wave propagation in the waveguide can be conveniently evaluated through the dynamic analysis of one unit cell (see Fig. 2) and the application of the Bloch theorem.

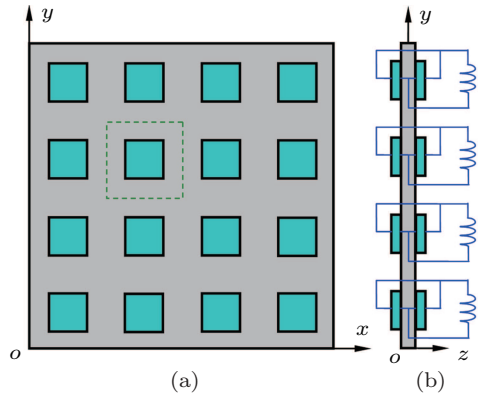


Fig. 1. (color online) (a) Substrate plate with arrays of piezo-patches. (b) Each pair of piezos connected to an inductive shunting circuit.

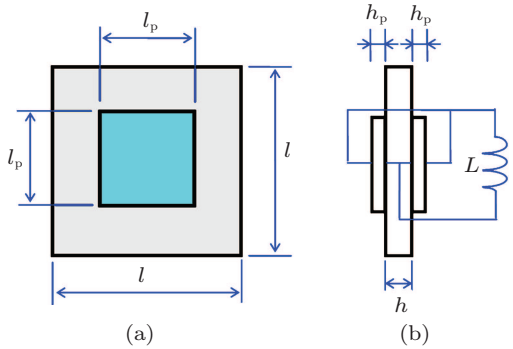


Fig. 2. (color online) Schematic of the unit cell: (a) top view and (b) side view.

2.2. Dynamics of unit cell in discretized format

The electromechanical model of the plate with surface-mounted piezo-patches is based on the stress-charge form of the constitutive equations for a piezoelectric material, which can be expressed as[17]

$$\begin{bmatrix} \boldsymbol{T} \\ \boldsymbol{D} \end{bmatrix} = \begin{bmatrix} \boldsymbol{c}^{\mathrm{E}} & -\boldsymbol{e}^{\mathrm{T}} \\ \boldsymbol{e} & \boldsymbol{\varepsilon}^{\mathrm{s}} \end{bmatrix} \begin{bmatrix} \boldsymbol{S} \\ \boldsymbol{E} \end{bmatrix}, \tag{1}$$

where $\boldsymbol{T}$ is the mechanical stress vector, $\boldsymbol{D}$ is the electric displacement vector, $\boldsymbol{S}$ is the mechanical strain vector, and $\boldsymbol{E}$ is the electric-field vector. Moreover, ε^{s} is the permittivity matrix at a constant strain, $\boldsymbol{e}$ is the matrix of piezoelectric stress constants, and $\boldsymbol{c}^{\mathrm{E}}$ is the stiffness matrix of the piezo-material at a constant electric field.

The combination of host plate and piezo-patches is modelled using 4-node Kirchhoff plate elements. Piezoelectric patches are polarized in the thickness direction, with electrodes connected to the top and bottom surfaces. Therefore, the discretized forms of the governing equations of the unit cell are derived by applying Hamilton's principle and standard finite element (FE) procedures, which give

$$\boldsymbol{M}_{uu}\ddot{\boldsymbol{d}} + \boldsymbol{K}_{uu}\boldsymbol{d} + \boldsymbol{K}_{\phi u}\phi = \boldsymbol{f}, \tag{2}$$

$$\boldsymbol{K}_{\phi u}\boldsymbol{d} + K_{\phi\phi}\phi = q, \tag{3}$$

where $\boldsymbol{d}$ is the vector of the nodal generalized displacements, $\boldsymbol{f}$ is the vector of the generalized forces, q is the total charge on the electrodes, and ϕ is the electric potential difference between the electrodes of each piezo-patch. Also, $\boldsymbol{M}_{uu}$, $\boldsymbol{K}_{uu}$, and $\boldsymbol{K}_{\phi u}$ are, respectively, the assembled mass, the stiffness, and coupling matrices. It is noteworthy that $K_{\phi\phi}$ is equal and opposite to the total capacitance of the piezo-pairs at a constant strain.

2.3. Modeling improvement

As each pair of piezo-patches is shunted by a single inductor, the relationship between ϕ and q can be given by

$$\phi = L\ddot{q}. \tag{4}$$

The conventional method to simplify Eqs. (2) and (3) is as follows.[19,20] First, under the assumption of the harmonic motion at frequency ω, equation (4) can be written as

$$q = -\frac{\phi}{\omega^2 L}. \tag{5}$$

Second, substituting Eq. (5) into Eq. (3) yields

$$\phi = -\left(\frac{1}{\omega^2 L} + K_{\phi\phi}\right)^{-1} \boldsymbol{K}_{\phi u}\boldsymbol{d}. \tag{6}$$

Then, substituting Eq. (6) into Eq. (2), the resulting form can be expressed as

$$\left[\boldsymbol{K}_{uu} - \omega^2 \boldsymbol{M}_{uu} - \boldsymbol{K}_{\phi u}\left(\frac{1}{\omega^2 L} + K_{\phi\phi}\right)^{-1} \boldsymbol{K}_{\phi u}\right]\boldsymbol{d} = \boldsymbol{f}. \tag{7}$$

As seen from Eq. (7), the resulting dynamic stiffness matrix is a complicated function of frequency, which cannot be reduced to a linear eigenvalue problem. Obviously, the nonlinear element is introduced by Eq. (6), so the reduction of it

needs to be improved. In order to solve this problem and obtain the dispersion relations through easy solution of a linear eigenvalue problem, we reduce Eqs. (2) and (3) as follows. First, equation (4) is not reduced into a nonlinear equation but substituted into Eqs. (2) and (3) directly, and the resulting equations can be rewritten as

$$\boldsymbol{M}_{uu}\ddot{\boldsymbol{d}}+\boldsymbol{K}_{uu}\boldsymbol{d}+\boldsymbol{K}_{\phi u}L\ddot{q}=\boldsymbol{f}, \tag{8}$$

$$\boldsymbol{K}_{\phi u}\boldsymbol{d}+K_{\phi\phi}L\ddot{q}=q. \tag{9}$$

Second, treating the total charge as a general nodal freedom and transforming Eqs. (8) and (9) into the following matrix form:

$$\boldsymbol{M}\ddot{\boldsymbol{u}}+\boldsymbol{K}\boldsymbol{u}=\boldsymbol{F}, \tag{10}$$

where $\boldsymbol{u}=\begin{bmatrix}\boldsymbol{d}\\ q\end{bmatrix}$, $\boldsymbol{F}=\begin{bmatrix}\boldsymbol{f}\\ 0\end{bmatrix}$ and

$$\boldsymbol{M}=\begin{bmatrix}\boldsymbol{M}_{uu} & \boldsymbol{K}_{\phi u}L\\ 0 & \boldsymbol{K}_{\phi\phi}L\end{bmatrix}\quad,\quad \boldsymbol{K}=\begin{bmatrix}\boldsymbol{K}_{uu} & 0\\ \boldsymbol{K}_{\phi u} & -1\end{bmatrix}, \tag{11}$$

and under the assumption of harmonic motion at frequency ω, equation (10) can be written as

$$\left(\boldsymbol{K}-\omega^2\boldsymbol{M}\right)\boldsymbol{u}=\boldsymbol{F}. \tag{12}$$

Obviously, contrary to Eq. (7), equation (12) gives a normal dynamic stiffness matrix that will lead to a linear eigenvalue problem that is easy to solve. Comparing the two modeling strategies, one can find that the critical improvement on this proposed method is to treat the charges on the patch as a general nodal freedom and increase the dimensionality of dynamic stiffness by one.

2.4. Bloch analysis

According to the locations of nodes shown in Fig. 3, the nodal displacement vector $\boldsymbol{u}$ can be partitioned into

$$\boldsymbol{u}=\left[\,\boldsymbol{d}_{\rm I}\ \boldsymbol{d}_{\rm B}\ \boldsymbol{d}_{\rm T}\ \boldsymbol{d}_{\rm L}\ \boldsymbol{d}_{\rm R}\ \boldsymbol{d}_{\rm LB}\ \boldsymbol{d}_{\rm RB}\ \boldsymbol{d}_{\rm LT}\ \boldsymbol{d}_{\rm RT}\ q\,\right]^{\rm T}, \tag{13}$$

$$\boldsymbol{F}=\left[\,0\ \boldsymbol{f}_{\rm B}\ \boldsymbol{f}_{\rm T}\ \boldsymbol{f}_{\rm L}\ \boldsymbol{f}_{\rm R}\ \boldsymbol{f}_{\rm LB}\ \boldsymbol{f}_{\rm RB}\ \boldsymbol{f}_{\rm LT}\ \boldsymbol{f}_{\rm RT}\ 0\,\right]^{\rm T}. \tag{14}$$

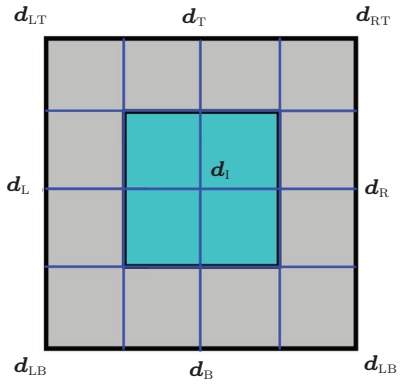


Fig. 3. (color online) Depiction of nine displacements in a square lattice.

The Bloch theorem in square lattice can be expressed as[29]

$$\begin{aligned}&\boldsymbol{d}_{\rm T}=\mathrm{e}^{\mathrm{i}k_yl}\boldsymbol{d}_{\rm B},\ \ \boldsymbol{d}_{\rm R}=\mathrm{e}^{\mathrm{i}k_xl}\boldsymbol{d}_{\rm L},\\ &\boldsymbol{d}_{\rm LT}=\mathrm{e}^{\mathrm{i}k_yl}\boldsymbol{d}_{\rm LB},\ \ \boldsymbol{d}_{\rm RB}=\mathrm{e}^{\mathrm{i}k_xl}\boldsymbol{d}_{\rm LB},\\ &\boldsymbol{d}_{\rm RT}=\mathrm{e}^{\mathrm{i}\left(k_x+k_y\right)l}\boldsymbol{d}_{\rm LB},\end{aligned} \tag{15}$$

$$\boldsymbol{f}_{\rm B}+\mathrm{e}^{-\mathrm{i}k_yl}\boldsymbol{f}_{\rm T}=0,\ \ \boldsymbol{f}_{\rm L}+\mathrm{e}^{-\mathrm{i}k_xl}\boldsymbol{f}_{\rm R}=0,$$
$$\boldsymbol{f}_{\rm LB}+\mathrm{e}^{-\mathrm{i}k_xl}\boldsymbol{f}_{\rm RB}+\mathrm{e}^{-\mathrm{i}k_yl}\boldsymbol{f}_{\rm LT}+\mathrm{e}^{-\mathrm{i}\left(k_x+k_y\right)l}\boldsymbol{f}_{\rm RT}=0, \tag{16}$$

where $\boldsymbol{k}=[k_x\ \ k_y]$ is the wave vector and $\mathrm{i}=\sqrt{-1}$.

The matrices forms of Eqs. (15) and (16) can be given by

$$\begin{aligned}&\boldsymbol{u}=\boldsymbol{T}\left(k_x,k_y\right)\hat{\boldsymbol{u}},\\ &\boldsymbol{T}^{\rm T}\left(-k_x,-k_y\right)\boldsymbol{F}=0,\end{aligned} \tag{17}$$

where $\hat{\boldsymbol{u}}=[\boldsymbol{d}_{\rm I}\ \ \boldsymbol{d}_{\rm B}\ \ \boldsymbol{d}_{\rm L}\ \ \boldsymbol{d}_{\rm LB}\ \ q]^{\rm T}$ and

$$\boldsymbol{T}\left(k_x,k_y\right)=\begin{bmatrix}\boldsymbol{I} & 0 & 0 & 0 & 0 & 0 & 0 & 0 & 0 & 0\\ 0 & \boldsymbol{I} & \boldsymbol{I}\mathrm{e}^{\mathrm{i}k_yl} & 0 & 0 & 0 & 0 & 0 & 0 & 0\\ 0 & 0 & 0 & \boldsymbol{I} & \boldsymbol{I}\mathrm{e}^{\mathrm{i}k_xl} & 0 & 0 & 0 & 0 & 0\\ 0 & 0 & 0 & 0 & 0 & \boldsymbol{I} & \boldsymbol{I}\mathrm{e}^{\mathrm{i}k_xl} & \boldsymbol{I}\mathrm{e}^{\mathrm{i}k_yl} & \boldsymbol{I}\mathrm{e}^{\mathrm{i}\left(k_x+k_y\right)l} & 0\\ 0 & 0 & 0 & 0 & 0 & & & & & 1\end{bmatrix}^{\rm T}. \tag{18}$$

The superscript T represents the transpose operator. Substitution of Eq. (17) into Eq. (12) can lead to

$$\left[\boldsymbol{S}_k\left(\boldsymbol{k}\right)-\omega^2\boldsymbol{I}\right]\hat{\boldsymbol{u}}=0, \tag{19}$$

where

$$\boldsymbol{S}_k\left(\boldsymbol{k}\right)=\frac{\boldsymbol{T}^{\rm T}\left(-k_x,-k_y\right)\times\boldsymbol{K}\times\boldsymbol{T}\left(k_x,k_y\right)}{\boldsymbol{T}^{\rm T}\left(-k_x,-k_y\right)\times\boldsymbol{M}\times\boldsymbol{T}\left(k_x,k_y\right)}. \tag{20}$$

Equation (14) can be solved to construct a band structure of wave frequency ω for a given wave vector $\boldsymbol{k}$. It is unnecessary to solve Eq. (19) for all values of $\boldsymbol{k}$. Due to the periodicity, all propagating modes are captured by restricting the wave vector to the irreducible Brillouin zone.[9]

3. Results and discussion

As an example, we choose epoxy (Young's modulus $E=4.35$ GPa, Poisson's ratio $\mu=0.37$, and density $\rho_{\rm b}=1180\ {\rm kg/m^3}$) as the material of host plate and PZT-5H as the material of piezo-patches. The geometrical parameters of the unit cell are summarized in Table 1, and the material properties of PZT-5H are listed in Table 2.

Table 1. Geometrical parameters of the unit cell.

l/mm	h/mm	l_p/mm	h_p/mm
80	5	40	0.2

Table 2. Material properties of PZT-5H.

Density/ $\mathrm{kg\cdot m^{-3}}$	s_{11}^{E}/ $\mathrm{/m^2\cdot N^{-1}}$	s_{12}^{E}/ $\mathrm{m^2\cdot N^{-1}}$	d_{31}/ $\mathrm{C\cdot N^{-1}}$	ε_{33}^{T}/ $\mathrm{F\cdot m^{-1}}$
7500	16.5×10^{-12}	-4.78×10^{-12}	-2.74×10^{-10}	3.01×10^{-8}

Based on the aforementioned FE method, band structures of the acoustic metamaterial are calculated with 144 FEs. Figure 4 shows the dispersion relations of the propagating waves with the values of inductance tuned at $L = 0$ and $L = 0.2$ H, respectively. When $L = 0$, no internal resonance will be induced in the shunting system and the dispersion curve is quite similar to that of a homogeneous plate in a frequency range of 0 Hz–700 Hz. By contrast, a complete gap separates the dispersion curves when L is chosen to be 0.2 H. The internal resonance of the inductive shunt is the dominant factor of the gap formation here. There is no simple formulation to predict the accurate resonant frequency, for the capacitance of the piezo-patch is related to its boundary conditions. However, the resonant frequency can be approximately estimated from

$$f = \frac{1}{2\pi\sqrt{LC}}, \quad C \in \left(2C_{\mathrm{p}}^{s}, 2C_{\mathrm{p}}^{\mathrm{T}}\right), \tag{21}$$

where $C_{\mathrm{p}}^{\mathrm{s}}$ and $C_{\mathrm{p}}^{\mathrm{T}}$ are the inherent capacitances of the piezo-patch at constant strain and stress, respectively.

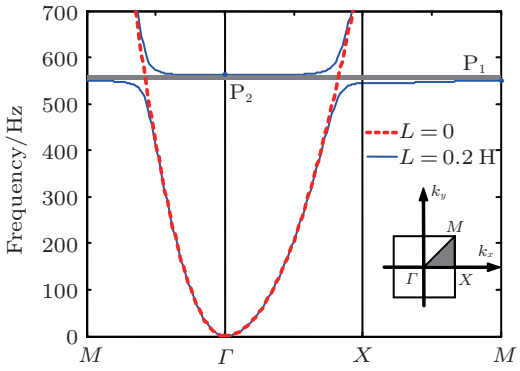


Fig. 4. (color online) Band structure along the edge of the irreducible Brillouin zone (shadowed region of inset).

The vibration modes of the unit cell corresponding to the edge frequencies (P_1 and P_2 in Fig. 4) of the band gap are shown in Fig. 5. The vibration mode at P_1 corresponds to the lower edge frequency where the phase difference between two adjacent cells is π as shown in Figs. 5(a) and 5(b). Both the host and piezo-patch show a considerable deformation, especially in the boundary regions of the peizo-patch. Moreover,

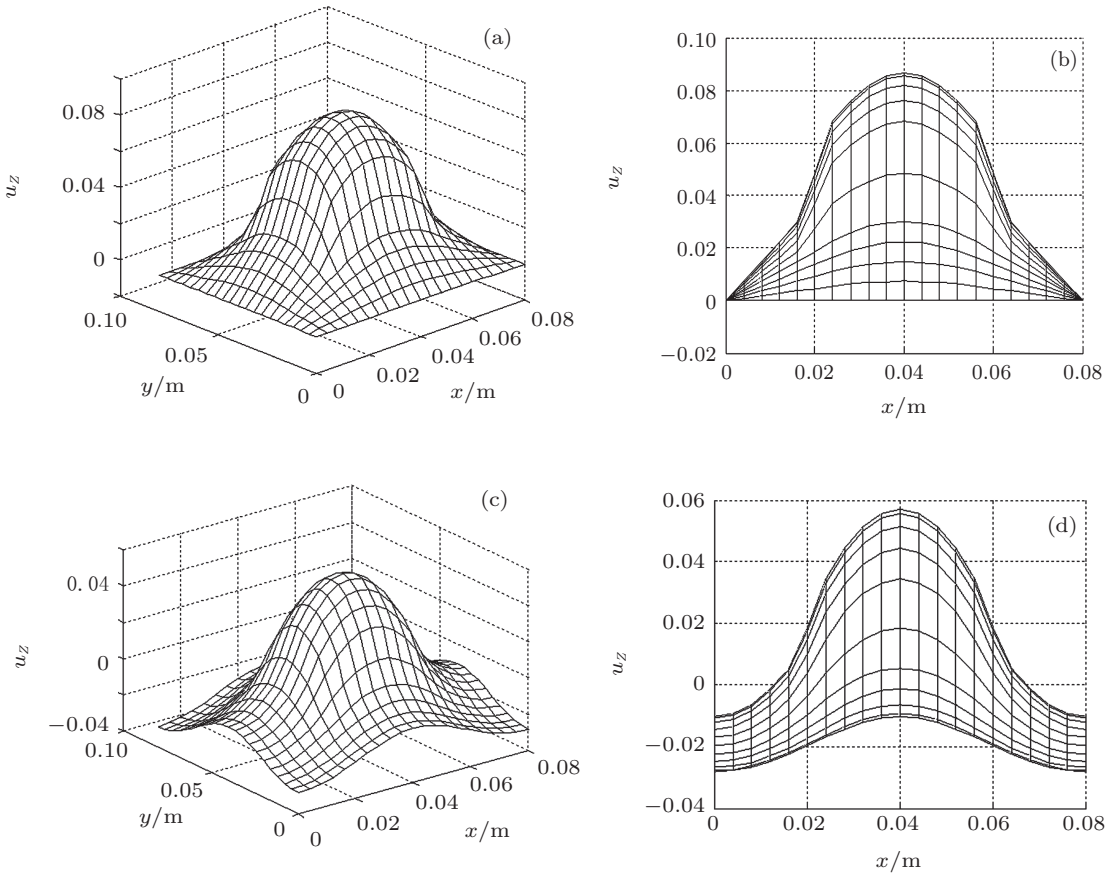


Fig. 5. Vibration modes of unit cell corresponding to edge frequencies of the band gap. Panels (a) and (b) show the isometric and side view of the mode shape at point P_1, and panels (c) and (d) exhibit the isometric and side view of the mode shape at point P_2.

the boundary conditions of each cell are equivalent to being completely clamped, i.e., the boundary frame keeps stationary. Compared with the vibration mode of the conventional LR sonic crystals, the vibration mode at point P_1 shows a notable difference, i.e., the vibrations at P_1 are not completely concentrated in the oscillators consisting of piezo-patches and shunting inductors. Actually, the complete LR modes existing in conventional LR PCs cannot occur in this inductive-shunted acoustic metamaterial, because the oscillators are strongly coupled with the host plate through piezo-patches and an oscillation can never exist in the circuits without mechanical deformations in piezo-patches. However, the oscillation between piezo-patch and inductive shunt is still the most dominant factor leading to the split of dispersion curves and band gap formation. The vibration mode at P_2 is similar to that at P_1 except that the vibrations in the host plate without piezos are more notable and in opposite phase to those in piezos as shown in Figs. 5(c) and 5(d). Contrary to the vibration mode at P_1, the boundary conditions of each cell at P_2 are equivalent to slides of the boundary frame.

Figure 6 shows the variations of bounding frequency with inductance. The bounding frequencies decrease with the increase of L, while the widths of the band gap vary little.

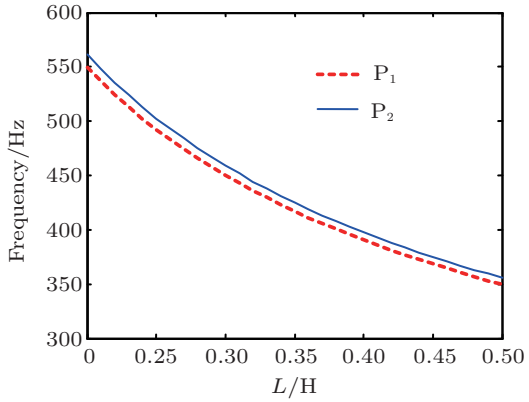


Fig. 6. (color online) Variations of bounding frequency at points P_1 and P_2.

4. Conclusions

In this paper, we propose an approach to circumvent a complicated dynamic stiffness matrix, which leads to a convenient solution for the dispersion properties of 2D waveguide with periodic arrays of resonant shunts. The results show that the internal resonances between inductive shunts and piezo-patches split the dispersion curves and form a resonant band gap. The band gap induced by resonant shunts is different from the conventional LR gap, for the vibrations are not completely localized in oscillators consisting of shunting inductors and piezo-patches. However, the oscillation of the shunting system is the dominant factor leading to the gap formation.

References

[1] Mead D J 1970 *J. Sound Vibr.* **11** 181
[2] Mead D J 1986 *J. Sound Vibr.* **104** 9
[3] Mead D J and Markus S 1983 *J. Sound Vibr.* **90** 1
[4] Kushwaha M S, Halevi P, Dobrzynski L and Djafari-Rouhani B 1993 *Phys. Rev. Lett.* **71** 2022
[5] Sigalas M 1998 *J. Appl. Phys.* **84** 3026
[6] Liu Z, Zhang X, Mao Y, Zhu Y Y, Yang Z, Chan C T and Sheng P 2000 *Science* **289** 1734
[7] Goffaux C, Sanchez-Dehesa J, Yeyati A L, Lambin P, Khelif A, Vasseur J O and Djafari-Rouhani B 2002 *Phys. Rev. Lett.* **88** 225502
[8] Wang G, Wen X, Wen J, Shao L and Liu Y 2004 *Phys. Rev. Lett.* **93** 154302
[9] Wang G, Wen J and Wen X 2005 *Phys. Rev. B* **71** 104302
[10] Fang J Y, Yu D L, Han X Y and Cai L 2009 *Chin. Phys. B* **18** 1316
[11] Wen J H, Yu D L, Xiao Y and Wen X S 2009 *Chin. Phys. B* **18** 2404
[12] Zhao H G, Wen J H, Liu Y Z, Yu D L, Wang G and Wen X S 2008 *Chin. Phys. B* **17** 1305
[13] Li J and Chan C T 2004 *Phys. Rev. E* **70** 055602
[14] Fang N, Xi D, Xu J, Ambati M, Strituravanich W, Sun C and Zhang X 2006 *Nature Mater.* **5** 452
[15] Milton G W 2007 *New J. Phys.* **9** 359
[16] Xiao Y, Wen J and Wen X 2012 *New J. Phys.* **14** 033042
[17] Thorp O, Ruzzene M and Baz A 2001 *Smart Mater. Struct.* **10** 979
[18] Thorp O, Ruzzene M and Baz A 2005 *Smart Mater. Struct.* **14** 594
[19] Airoldi L and Ruzzene M 2011 *J. Intell. Mater. Syst. Struct.* **10** 979
[20] Airoldi L and Ruzzene M 2011 *New J. Phys.* **13** 113010
[21] Chen S, Wen J, Wang G, Yu D and Wen X 2012 *J. Intell. Mater. Syst. Struct.* **23** 1613
[22] Wang G, Chen S and Wen J 2011 *Smart Mater. Struct.* **20** 015026
[23] Chen S B, Han X Y, Yu D L and Wen J H 2010 *Acta Phys. Sin.* **59** 387 (in Chinese)
[24] Chen S B, Wen J H, Yu D L, Wang G and Wen X S 2011 *Chin. Phys. B* **20** 014301
[25] Chen S B, Wen J H, Wang G, Han X Y and Wen J H 2011 *Chin. Phys. Lett.* **28** 094301
[26] Wang G, Wang J and Chen S 2011 *Smart Mater. Struct.* **20** 125019
[27] Spadoni A, Ruzzene M and Cunefare K A 2009 *J. Intell. Mater. Syst. Struct.* **20** 979
[28] Casadei F, Ruzzene M, Dozio L and Cunefare K A 2010 *Smart Mater. Struct.* **19** 015002
[29] Farzbod F and Leamy M J 2009 *J. Sound Vibr.* **325** 545